PHYSICAL REVIEW B VOLUME 44, NUMBER 6 1 AUGUST 1991-II

Suppression of phase-locking chaos in long Josephson junctions by biharmonic microwave fields

Mario Salerno
Dipartimento di Fisica Teorica, Università di Salerno, 84100 Salerno, Italy
(Received 28 December 1990)

We consider the problem of phase locking of fluxon oscillations in long Josephson junctions irradiated by an external microwave field consisting of two harmonic signals, one at frequency ω and the other at frequency $\omega/2$ added together (biharmonic driver). The analysis is performed in terms of a two-dimensional map constructed in terms of the fluxon time of flight and fluxon's energy inside the junction. As a result we find that the second driver enhances the stability of the phase-locking state and can be used to suppress the phase-locking chaos in the middle of the step induced by the first driver.

I. INTRODUCTION

In some previous papers we have described the phase-locking phenomenon observed in long Josephson junctions, in the presence of an external microwave field, in terms of a two-dimensional map for the time of flight and the fluxon energy inside the junction.[1–3] Such a map reduction was achieved under the assumption that the motion of a single fluxon inside the junction couples to the microwave field through boundary conditions. By using this approach it was shown that an external harmonic driver can induce the phase-locked dynamics on a subharmonic step to be chaotic through a cascade of period-doubling bifurcations.[3] The aim of the present paper is to extend this analysis to the case in which the junction is irradiated by a biharmonic driver, i.e., a driver consisting of two harmonic fields, one of frequency ω and another of frequency $\omega/2$, added together. In the context of small Josephson junctions, subharmonic drivers were shown to stabilize fixed points against bifurcation.[4–8] Here, in the long Josephson junctions case, we find that the $\omega/2$ driver splits the fixed point corresponding to the fluxon equal time-of-flight dynamics into two stable fixed points, one of which is physically more relevant (it has larger stability domains in current and larger basin of attraction). We show that, by increasing the amplitude of the subharmonic signal, the stability of this stable fixed point is enhanced, and quite surprisingly, the chaos generated by the first driver in the central portion of the step[3] is suppressed. We think that this chaos suppression phenomenon is of general validity and we expect it to be observed in other systems too. The paper is organized as follows. In Sec. II, we introduce the system and we briefly sketch the derivation of the phase-locking map for a junction of in-line geometry[9] in the presence of a biharmonic driver. In Sec. III, we study the existence of the fixed points of such a map and find the range of locking in the current as a function of the amplitudes of the two rf fields. Moreover, by studying the linearized map, we show that the stability of the physically relevant fixed point is enhanced by the $\omega/2$ driver and that this stabilization can be used to destroy chaos. In Sec. IV, we compare these results with those obtained by numerical iterations of the map, and finally, in Sec. V, we summarize the main results of the paper.

II. THE MAP MODEL

We briefly sketch the derivation of the map model, referring for more details to Refs. [1–3]. Let us start by recalling that the electrodynamics of a long Josephson junction of in-line geometry[9] is described by the damped sine-Gordon equation in normalized form (for details on normalizations see Ref. 2)

$$\phi_{xx}-\phi_{tt}-\sin\phi=\alpha\phi_t \tag{1}$$

with boundary conditions

$$\begin{aligned}\phi_x(0,t)&=\kappa+\eta(t)\ ,\\ \phi_x(L,t)&=-\kappa+\eta(t)\ .\end{aligned} \tag{2}$$

Here L denotes the normalized length of the junction, κ is a constant representing the dc bias current through the junction, and $\eta(t)$ is a time-dependent magnetic field of the form

$$\eta(t)=\eta_1\cos(\omega t+\vartheta)+\eta_2\cos\left[\frac{\omega}{2}t+\vartheta\right]\ , \tag{3}$$

modeling the external microwave field. We distinguish between magnetic and electric couplings according to whether we change the signs of both η_1 and η_2 at the ends of the junction or not. In the following, however, we consider only the case of electric coupling (the results are easily generalizable to the case of magnetic coupling as well). The dynamics of a single fluxon inside the junction can be described by the perturbation theory of McLaughlin and Scott.[10] Following these authors, we find, for the fluxon momentum,

$$\frac{dP}{dt}=-\alpha P\ , \tag{4}$$

from which the trajectory of the fluxon inside the junction is readily obtained,[11]

$$X(t)=X_0+\alpha^{-1}[\sinh^{-1}z_0-\sinh^{-1}(z_0e^{-\alpha(t-t_0)})]\ , \tag{5}$$

where z_0 denotes the reduced momentum $P/8$ evaluated at time t_0. By inverting Eq. (5) and imposing $X-X_0=L$, we obtain, for the time required by the fluxon to transverse the junction,

$$T_{k+1}-T_k=\alpha^{-1}\ln\left[\frac{(U_k^2-1)^{1/2}}{C(U_k^2-1)^{1/2}-SU_k}\right], \tag{6}$$

where $C=\cosh(\alpha L)$, $S\equiv\sinh(\alpha L)$, U is the reduced fluxon energy $U\equiv H/8=(1-\dot{X})^{-1/2}$, and we used subscripts k's to denote the value at the kth reflection. At the edges of the junction the fluxon is kicked by the boundary terms (2) and (neglecting the losses during the reflection) its energy changes according to

$$\Delta U=\frac{\pi}{2}[\kappa+\eta(t)]\ . \tag{7}$$

From Eq. (7) we obtain a relation between U_k and U_{k+1},

$$U_{k+1}=CU_k-S(U_k^2-1)^{1/2}+\frac{\pi}{2}\left[\kappa+\eta_1\cos(\omega T_{k+1})+\eta_2\cos\left[\frac{\omega}{2}T_{k+1}\right]\right], \tag{8}$$

which, together with Eq. (6), constitute a two-dimensional map of the half-cylinder $S^1\times\mathbb{R}^+$ into itself (note that the T variable is periodic with period $4\pi/\omega$). Fixed points of this map corresponding to phase-locked dynamics of the fluxon inside the junction, are studied in the next section.

III. EXISTENCE AND STABILITY OF FIXED POINTS

The equal time of flight fixed points are easily found in the following manner. We insert the locking condition

$$T_{k+1}-T_k=\frac{m\pi}{\omega} \tag{9}$$

into Eq. (6) and solve the resulting equation for U as

$$U^*=\frac{C-E}{[(C-E)^2-S^2]^{1/2}}\ , \tag{10}$$

where $E\equiv\exp(-m\pi\alpha/\omega)$ and m denotes the subharmonic order. By substituting this expression into Eq. (8) and imposing the fixed-point condition $U_{k+1}=U_k=U^*$, we obtain

$$T_\pm=\frac{2}{\omega}\cos^{-1}\left[-\frac{\eta_2}{4\eta_1}\pm\left[\left[\frac{\eta_2}{4\eta_1}\right]^2+\frac{\bar{\kappa}+\eta_1-\kappa_0}{2\eta_1}\right]^{1/2}\right], \tag{11}$$

where

$$\bar{\kappa}\equiv\frac{2(C-1)(1+E)}{\pi(1-2EC+E^2)^{1/2}} \tag{12}$$

represents the value of the bias current at which the rf-induced step intersects the unperturbed ($\eta_1=0$, $\eta_2=0$) zero-field step. We note that $T_+\in[0,\pi/\omega]$ while $T_-\in[\pi/\omega,2\pi/\omega]$ so that the equal time of the flight fixed points is given by

$$T_1^*\equiv(U^*,T_+),\quad T_2^*\equiv(U^*,T_-) \tag{13}$$

together with the ones obtained from these by reflection, respectively, around $4\pi/\omega$ and $2\pi/\omega$, i.e.,

$$T_4^*\equiv(U^*,4\pi/\omega-T_+),\quad T_3^*\equiv(U^*,2\pi/\omega+T_-)\ . \tag{14}$$

As a difference from the case of the single harmonic driver considered in Refs. 2 and 3, we have four possible values (instead of two) of the phase of the driving signal for which the equal time of flight solution is possible. Furthermore, when $\eta_2=0$, we see from Eq. (11) that these values exactly reduce to the ones derived in Refs. 2 and 3. The ranges of bias current for which the fixed points T_1^*, T_4^*, and T_2^*, T_3^* exist are, respectively, derived from Eq. (11) as

$$\bar{\kappa}-\eta_1-\eta_2\le\kappa\le\bar{\kappa}+\eta_1+\frac{\eta_2^2}{8\eta_1} \tag{15}$$

and

$$\bar{\kappa}-\eta_1+\eta_2\le\kappa\le\bar{\kappa}+\eta_1+\frac{\eta_2^2}{8\eta_1}\ , \tag{16}$$

from which we note that they are different and asymmetric with respect to the point $\kappa=\bar{\kappa}$. Furthermore, when $\eta_2=0$, these ranges coincide and the asymmetry disappears, in agreement with the results of Refs. 2 and 3. The stability of these fixed points is studied in terms of the Jacobian matrix of the mapping evaluated at U^*, T^*,

$$\mathcal{J}=\begin{bmatrix}1 & -\dfrac{\sinh(\alpha L)\xi}{\alpha}\\ -\gamma(T^*) & E-\dfrac{\gamma(T^*)}{\alpha}\end{bmatrix}, \tag{17}$$

where

$$\gamma(x)=\frac{\pi}{2}\frac{d\eta(x)}{dx},\quad \xi=(U^*-1)^{-3/2}E\ .$$

By requiring that all the eigenvalues of $\mathcal{J}$ are in the unit circle, we get, as a sufficient condition for the stability,

$$0\ge\eta_1\sin(\omega T_i^*)+\frac{\eta_2}{2}\sin\left[\frac{\omega T_i^*}{2}\right]\ge-\Lambda\ , \tag{18}$$

where $i=1$, 2, 3, and 4, and

$$\Lambda=\frac{4\alpha E(1+E)\sinh^2(\alpha L)}{\pi\omega[1-2E\cosh(\alpha L)+E^2]^{3/2}}\ . \tag{19}$$

From Eq. (18) we see that the left inequality in Eq. (18) can never be satisfied for T_1^*, while it is always satisfied for T_4^*. This implies that T_1^* is always unstable while T_4^* is stable if the right inequality is also fulfilled. For T_2^*, T_3^* we have a more complicated situation since, depending on the ratio η_1/η_2, we may have T_2^* stable and T_3^* unstable or vice versa. For simplicity, in the following we restrict ourselves to the case in which the amplitude η_2 of the subharmonic driver is smaller than η_1. In this case, from Eq. (18) it follows that the only stable fixed points corresponding to the equal time-of-flight solution are given by T_2^* and T_4^*. In Fig. 1 we have reported the ranges of stability in current, as derived from Eq. (18), versus η_2 for the fixed points T_2^* and T_4^* and for parameter values $L=12$, $\alpha=0.05$, $m=8$, $\eta_1=0.21$. The vertical continuous intervals ranging from $\eta_2=0$ to $\eta=0.18$ in in-

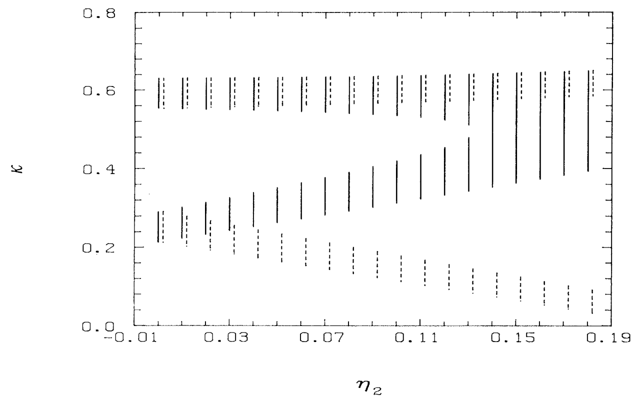

FIG. 1. Intervals of stability in current as derived from Eq. (18) for the fixed points T_2^* (solid intervals) and T_4^* (dashed intervals) for parameter values $L=12$, $\alpha=0.05$, $\omega=1.5$, $m=8$, $\eta_1=0.21$, and for η_2 values ranging from $\eta_2=0$ (right most interval) to $\eta_2=0.18$ by increments of 0.01. The dashed intervals are shifted by 0.002 along the η_2 axis in order to avoid overlapping.

crements of 0.01 refer to the fixed point T_2^* while the corresponding dashed ones, referring to T_4^*, have been shifted by 0.002 along the η_2 axis in order to avoid overlapping. We see that the upper and lower ends of these intervals coincide with the corresponding limiting values given by Eqs. (15) and (16), and the onset of instability is at the center of the step. Furthermore, violation of inequality (18) first occurs at κ values for which the eigenvalues of the Jacobian matrix leaves the unit circle at -1 along the negative real axis. This implies that the fixed point loses stability in a flip bifurcation with the birth of a stable period-2 orbit. The internal ends of the intervals in Fig. 1 represent the current values at which bifurcations occur. From this figure we also see that when $\eta_2=0$, the ranges of stability in current of the two fixed points coincide, being, in this limit, $T_2^* \equiv T_4^*$. By increasing η_2, the two intervals of stability relative to the fixed point T_4^* move apart and the instability region in the center is increased, while for T_2^* they merge into a single interval shrinking to zero the instability region in the middle. This suggests that, on the step corresponding to the fixed point T_2^*, the second driver can be used to reduce (eventually destroy) the chaotic behavior observed in the middle of subharmonic steps and reported in Ref. 3. For the step corresponding to T_4^*, the situation is just the opposite, i.e., the biharmonic microwave field enhances the instability in center of the step. On the other hand, from Fig. 1 we see that the fixed point T_4^* has ranges of stability in current smaller than the ones relative to T_2 and, by increasing η_2, the upper stability branch of T_4^* overlaps with the stability range of T_2^*. From this we may expect that, when T_4^* becomes unstable, the system switches over to the more stable fixed point T_2^* and no intrinsic instability (chaos) will be in the system. As to the lower stability branches of T_4^* in Fig. 1, we expect them to be physically less interesting since, by increasing η_2, they go down in the current region where the fluxon's oscillations may be stopped or destroyed by the external field. These should correspond to phase-locked states which are observable only by a fine scanning on initial conditions. In the next section we compare these results with the one obtained by numerical iterations of the map.

IV. NUMERICAL RESULTS

By direct iterations of the map (6) and (7), we construct the I-V characteristic of the junction by computing, for a given value of the dc current κ, the average voltage defined as

$$\langle V \rangle = 2\pi / \langle T_F \rangle \ .$$

Here T_F denotes the fluxon time of flight directly calculated from the map as $T_F \equiv T_{k+1} - T_{k-1}$. In Fig. 2 we report a typical current-voltage characteristic for the case of locking at a subharmonic frequency. The smooth curve in this figure represents the current-voltage characteristic (zero-field step) in the absence of external signals, while the discontinuous one represents a subharmonic step of order $m=8$ induced by a biharmonic driver with amplitudes $\eta_1=0.18$, $\eta_2=0.01$, and $\omega=1.5$. The parameters of the junction are fixed, here and in the following, to be $L=12$, $\alpha=0.05$, and the average voltage is computed over the first 100 iterations of the map after 300 free iterations. The step in Fig. 2 corresponds to the fixed point T_2^* and its extension in the current agrees well with the analytic prediction of Eq. (16). According to stability analysis, this point loses stability in a flip bifurcation at two values of the current determined by Eq. (18) (see the solid intervals in Fig. 1). In Fig. 3 we reported the bifurcation diagram for the time $T_L \equiv T_{k+1} - T_k$ required by the fluxon to transverse the junction versus κ as the bifurcation parameter κ is varied along the step of Fig. 2. In

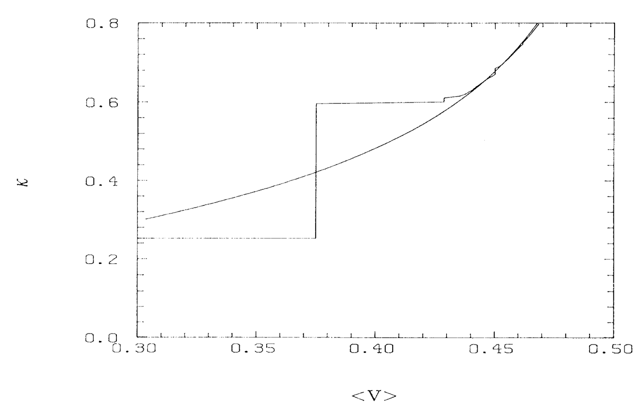

FIG. 2. Current-voltage characteristic referring to the fixed point T_2^* for a junction with parameters $L=12$, $\alpha=0.05$, and in the presence of a biharmonic field with $\eta_1=0.18$, $\eta_2=0.01$, $\omega=1.5$. The solid curve denotes the unperturbed zero-field step while the discontinuous one represents a subharmonic step of order $m=8$

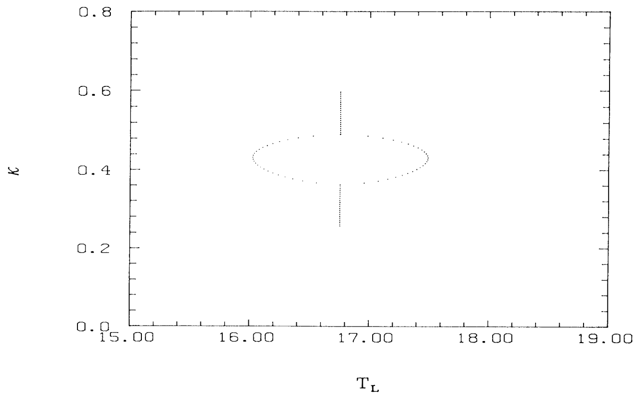

FIG. 3. Bifurcation diagram for $T_L \equiv T_{k+1} - T_k$ vs κ as κ is varied along the step of Fig. 2. The parameters are the same as in Fig. 2.

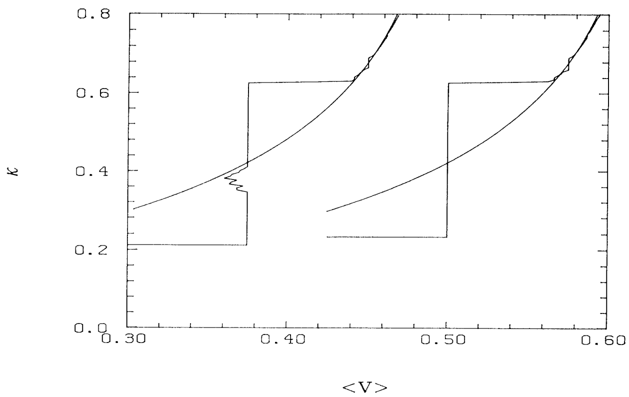

FIG. 4. Current-voltage characteristics as in Fig. 2 but for $\eta_1=0.21$ and η_2, respectively, 0 (left-hand curve) and 0.02 (right-hand curve). There is an offset of 0.125 between the two curves along the $\langle V \rangle$ axis in order to avoid overlapping.

Table I we reported the analytical and the numerical values of these bifurcation points for different values of η_2 and for $\eta_1=0.18$, from which we see that they agree well up to three significant digits. Furthermore, we note that the range of existence of the period-2 solution rapidly decreases with increasing values of η_2 in agreement with the results of Fig. 1. This stabilization against bifurcation becomes more important at higher values of η_1 where chaotic dynamics may become possible.[3] In Fig. 4 we show two sets of current voltage characteristics for a junction driven by a biharmonic field with $\eta_1=0.21$ and η_2, respectively, given by $\eta_2=0$ (left curves) and $\eta_2=0.02$ (right curves). In this figure the second set of curves was shifted by 0.125 along the voltage axis in order to avoid overlapping. The continuous curves denote the unperturbed zero-field step, while the discontinuous ones are subharmonic steps of order $m=8$. We see that when $\eta_2=0$, the voltage wanders from the phase-locked value over the central portion of the step, while, when $\eta_2=0.01$, the step is perfectly vertical. In Fig. 5 we report the bifurcation diagram T_L versus κ for $\eta_1=0.21$ and $\eta_2=0$. From this figure it is evident that the breakdown of phase locking in the central portion of the step of Fig. 4 ($\eta_2=0$ curve) is due to the appearance of chaos. This result is confirmed by the power spectra analysis of the time sequence T_L as reported in Ref. 3. In Fig. 6 we reported similar bifurcation diagrams to those in Fig. 3 for increasing values of η_2 starting from $\eta_2=0.02$ (left most curve) up to $\eta_2=0.14$ (right most curve), in increments of 0.02. (In order to avoid overlapping, an offset of 3 between the diagrams was introduced along the T_L axis.) We see that the period-doubling cascade from order to chaos and the corresponding reversed one, from chaos to order, shown in Fig. 3, disappear when we increase the amplitude of the subharmonic driver. At the value $\eta_2=0.14$, no bifurcations are present and the equal time-of-flight solution is stable in the whole range of existence. We see that the stabilization against bifurcation of the fixed point T_2^* induced by the subharmonic driver shrinks to zero the instability portion of the step and, as a consequence, the chaos in the central portion is suppressed. This is in agreement with the results predicted by Eq. (18) as also seen from a comparison between Fig. 4 and Fig. 1 (solid intervals). This chaos suppression induced by the subharmonic signal we expect to be of general validity for systems in which the transition from regular to chaotic behavior is approached through period doubling. As to the fixed point T_4^*, we have reported in Fig. 7 the corresponding $m=8$ subharmonic step induced by a biharmonic field with $\eta_1=0.21$, $\eta_2=0.03$, and $\omega=1.5$. The step on the left-hand side in Fig. 7 was obtained by using, as initial conditions for T and U, the ones corresponding to the fixed point T_4^* evaluated at the bottom of the step ($\kappa=\bar{\kappa}-\eta_1-\eta_2$) and iterating the map for increasing values of κ while the step on the right-hand side was obtained by starting with initial conditions T_4^* at the top of the step and by decreasing κ (the step on the right-hand side is shifted by 0.125 along the $\langle V \rangle$ axis to avoid overlapping). From this figure we see the presence of hysteresis at the bottom, due to the existence of two fixed points T_2^*, T_4^* both simultaneously stable in that current region (see Fig. 1). In Fig. 8 we have on the right-hand side and on the left-hand side the corresponding bifurcation diagram for the steps in Fig. 7 (the dia-

TABLE I. Numerical and analytical bifurcation values relative to the fixed point T_2^* for different values of η_2 and with $\eta_1=0.18$, $\omega=1.5$, $L=12$, $\alpha=0.05$.

η_2	$\kappa_{1\,\mathrm{an}}$	$\kappa_{1\,\mathrm{num}}$	$\kappa_{2\,\mathrm{an}}$	$\kappa_{2\,\mathrm{num}}$
0.00	0.3480	0.3476	0.4945	0.4941
0.01	0.3630	0.3628	0.4900	0.4897
0.02	0.3790	0.3786	0.4845	0.4848
0.03	0.3970	0.3966	0.4770	0.4774
0.04	0.4210	0.4207	0.4645	0.4649

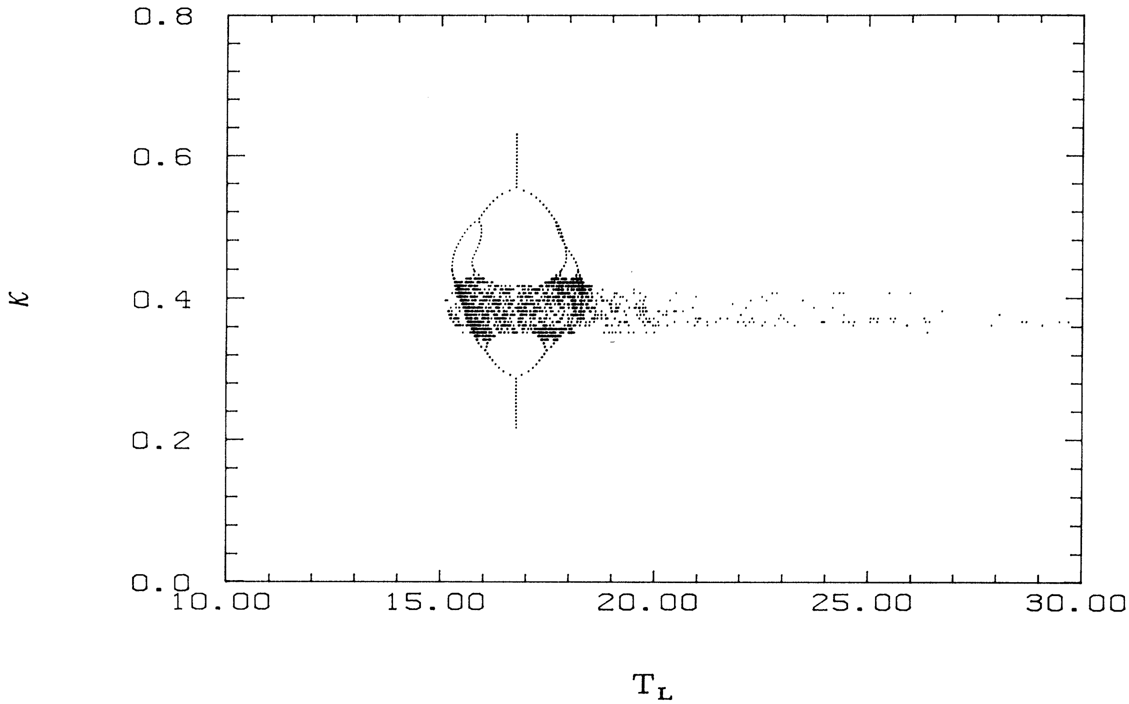

FIG. 5. Same as in Fig. 3 but for $\eta_1=0.21$, $\eta_2=0$, and κ is varied along the $\eta_2=0$ characteristic of Fig. 4.

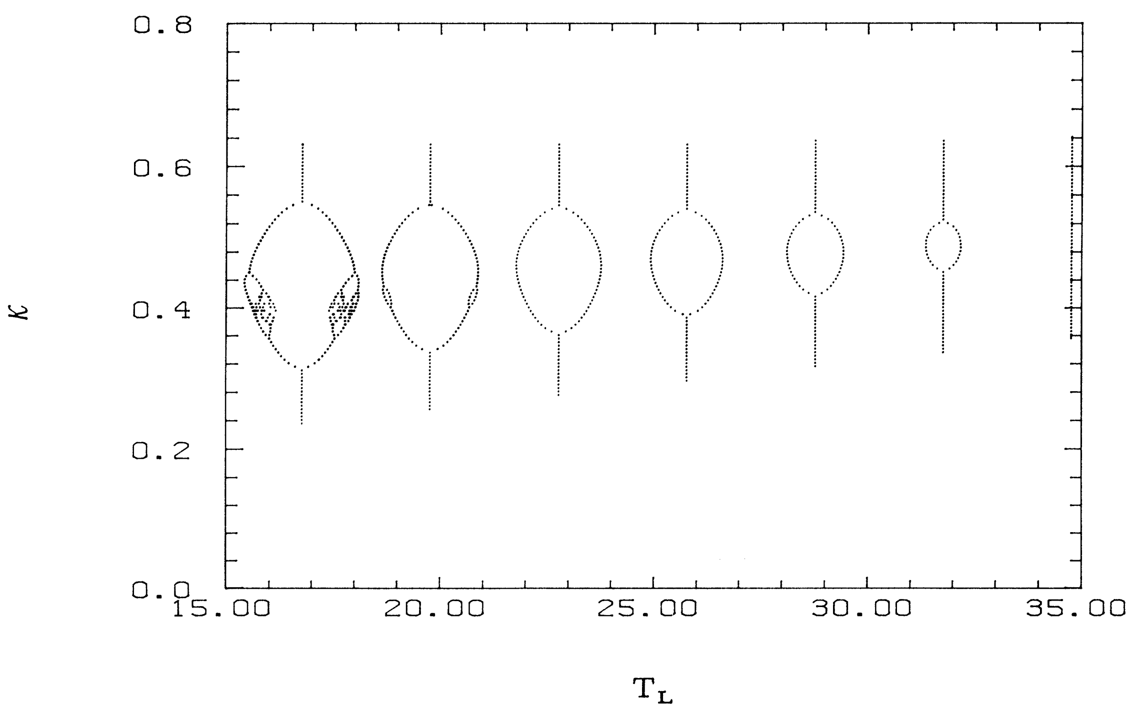

FIG. 6. Bifurcation diagrams as in Fig. 5 for increasing values of η_2 from $\eta_2=0.02$ (left most diagram) to $\eta_2=0.14$ (right most diagram) in increments of 0.02. To avoid overlapping, an offset of 3 between the diagrams was introduced along T_L.

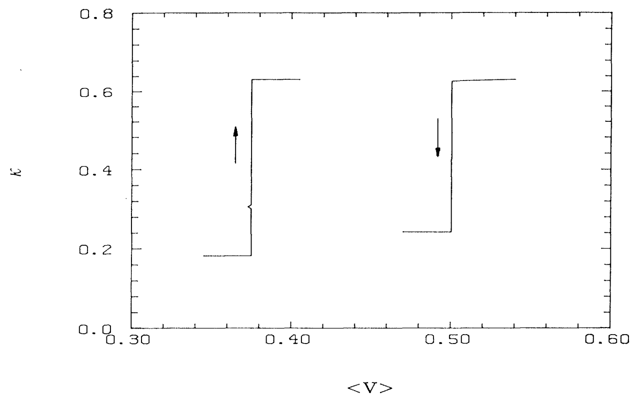

FIG. 7. Current-voltage characteristics obtained by taking, as initial conditions, the fixed point T_4^* evaluated, respectively, at the bottom (left-hand step) and at the top (right-hand step). The arrows indicate the verse in which the current is successively varied. The parameter values were fixed to $\eta_1=0.21$, $\eta_2=0.03$, $\omega=1.5$, $L=12$, $\alpha=0.05$, and the right-hand step has been shifted by a 0.125 along the $\langle V \rangle$ axis.

gram on the left-hand side is shifted by $4\pi/\omega$ along the T axis), from which it is clear that, by varying the current along the steps, at some point in the bifurcation cascade relative to the fixed-point T_4^* one switches over the other stable fixed point (horizontal arrows indicate the jump, the other arrows denote the verse in which the current is changed). We also see that this switchover corresponds, in the current voltage characteristic, to the little bump on the left step of Fig. 7 (on the other step it is not visible). We can therefore conclude that, as consequence of the overlapping of the stability domains of the fixed points for small values of η_2 (see Fig. 1), the corresponding steps look very similar. By increasing η_2, the overlapping will be only on the top of the step while at the bottom there will be a small vertical portion of the step corresponding to the dashed lower branches of Fig. 1. By increasing η_2 these small vertical steps go down in current at values for which the fluxon can stop or can be destroyed by the driver, therefore they can be seen only by properly choosing the initial conditions. From this point of view they appear physically less important.

V. CONCLUSIONS

We have shown that the addition of a small subharmonic signal of frequency $\omega/2$ to the fundamental driver (biharmonic driver) enhances the stability of phase-locking states in long Josephson junctions and can be used to suppress the chaos appearing in the middle of a subharmonic step. This result is of particular importance in practical applications of the phase-locked Josephson oscillator since it gives the possibility to eliminate the

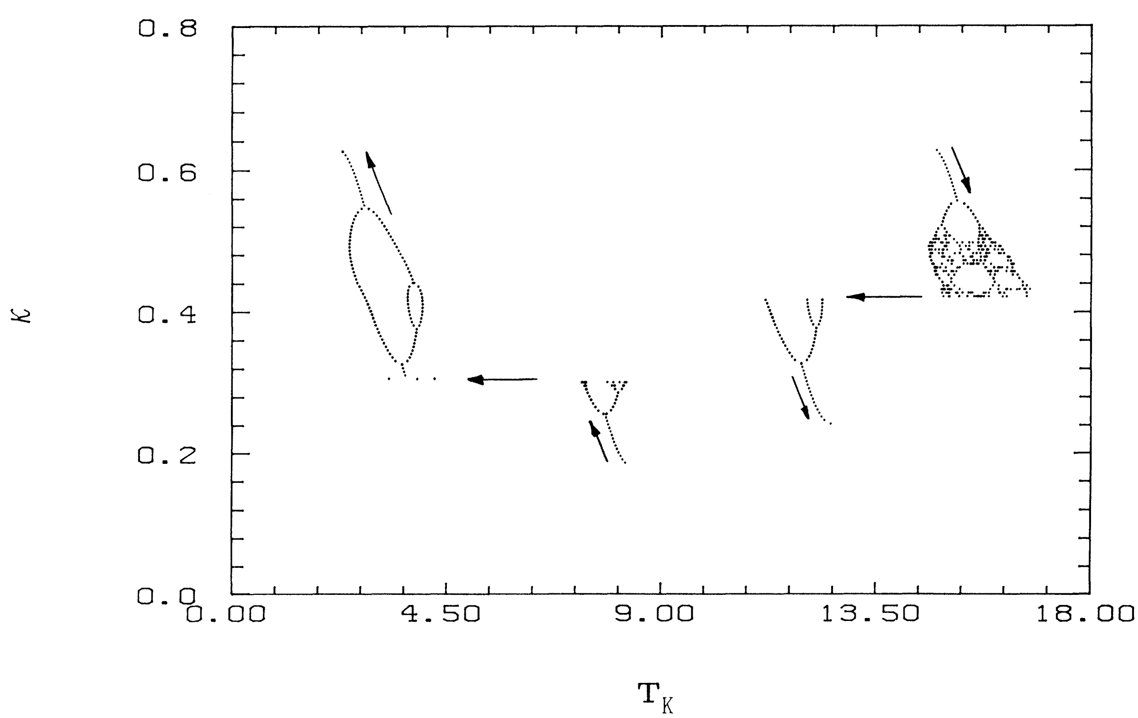

FIG. 8. Bifurcation diagrams for the phase T_k vs κ relative to the steps of Fig. 7. The left-hand diagram corresponds to the left-hand step in Fig. 7 and the right-hand diagram has been shifted by $4\pi/\omega$ along the T_k axis. The vertical arrows denote the verse in which the current is varied while the horizontal ones denote the value of κ at which the system jumps over the bifurcation tree relative to the fixed point T_2^*.

deterministic noise when operating on subharmonic steps. Finally, we remark that this chaos suppression by biharmonic drivers is a phenomenon that extends to all systems which have a transition from order to chaos via period doubling. Further work in this direction is presently in progress.

ACKNOWLEDGMENTS

This work profited from a fruitful discussion with Mogens Samuelsen. Financial support from (GNSM-CISM-INFM) Istituto Nazionale Fisica della Materia, Italy is acknowledged.

[1] M. Salerno, M. R. Samuelsen, G. Filatrella, S. Pagano, and R. D. Parmentier, Phys. Lett. A **137**, 75 (1989).

[2] M. Salerno, M. R. Samuelsen, G. Filatrella, S. Pagano, and R. D. Parmentier, Phys. Rev. B **41**, 6641 (1990).

[3] M. Salerno, Phys. Lett. A **144**, 453 (1990).

[4] H. Svensmark and M. R. Samuelsen, Phys. Rev. B **41**, 4181 (1990).

[5] K. Wiesenfeld and B. McNamara, Phys. Rev. Lett. **55**, 13 (1985).

[6] K. Wisenfeld and B. McNamara, Phys. Rev. A **33**, 629 (1986).

[7] P. Bryant and K. Wiesenfeld, Phys. Rev. A **33**, 2525 (1986).

[8] K. Wiesenfeld, J. Stat. Phys. **28**, 1071 (1985).

[9] A. Barone and G. Paterno, *Physics and Application of the Josephson Effect* (Wiley, New York, 1982), Chap. 5.

[10] D. W. McLaughlin and A. C. Scott, Phys. Rev. A **18**, 1652 (1978).

[11] O. A. Levring, N. F. Pedersen, and M. R. Samuelsen, J. Appl. Phys. **54**, 987 (1983).